applied sciences

MDPI

Article

A Logistics UAV Parcel-Receiving Station and Public Air-Route Planning Method Based on Bi-Layer Optimization

Honghai Zhang, Fei Wang, Dikun Feng, Sen Du, Gang Zhong *, Cheng Deng and Ji Zhou

College of Civil Aviation, Nanjing University of Aeronautics and Astronautics, Nanjing 210016, China
* Correspondence: zg1991@nuaa.edu.cn

Abstract: The popularity of unmanned aerial vehicle (UAV) technology has made UAV logistics transportation possible. However, based on the current development status of logistics UAVs, there are difficulties in using UAVs directly for door-to-door logistics transportation. Therefore, it is necessary to establish UAV parcel-receiving stations that can gather logistics needs in a small area. The construction of stations allows the UAVs to transport back and forth between the distribution warehouse and the established stations, enabling customers to send and receive packages at the more convenient stations. Based on the current situation, it is a more appropriate air–ground cooperative transport mode to solve the "last-mile" cargo transportation problem. In this paper, a bi-layer UAV parcel-receiving station and public air-route planning method is proposed to explore the interaction between station location and public route planning, and is solved with a genetic algorithm and max–min ant system (GA-MMAS). The model proposed in this paper can determine the location of the stations and plan the public air routes between the warehouse and stations simultaneously. Simulation results show that the planning results of the bi-layer optimization model proposed in this paper meet the requirements of station location and public air-route planning. Compared with the layered planning results, the cost of the upper-layer model is reduced by 5.12% on average, and the cost of the lower-layer model is reduced by 4.48%.

Keywords: logistics UAV; location problem; public air route; bi-layer optimization

check for updates

Citation: Zhang, H.; Wang, F.; Feng, D.; Du, S.; Zhong, G.; Deng, C.; Zhou, J. A Logistics UAV Parcel-Receiving Station and Public Air-Route Planning Method Based on Bi-Layer Optimization. *Appl. Sci.* **2023**, *13*, 1842. https://doi.org/10.3390/app13031842

Academic Editors: Shanling Dong and Meiqin Liu

Received: 28 December 2022
Revised: 26 January 2023
Accepted: 30 January 2023
Published: 31 January 2023

1. Introduction

With the rapid development of artificial intelligence, unmanned aerial vehicles (UAVs) have gradually come into the public's view. Their low costs and high mobility make UAVs have great development potential in many fields [1]. At the same time, with the advent of the Internet era, online shopping has become more popular, and the demand for logistics distribution is also growing. However, due to the scattered destinations of logistics transportation, the door-to-door distribution mode consumes many resources at the end of the transportation chain. Therefore, it is urgent to explore the potential of low-altitude airspace and improve "last-mile" cargo transportation [2].

Based on the development status of logistics UAVs, there are certain difficulties in infrastructure construction and operation management of logistics UAV door-to-door distribution. Therefore, this paper proposes a UAV air–ground cooperative transport mode. Parcel-receiving stations are set up in the demand-intensive area so that UAVs can transport goods between the distribution warehouse and the parcel-receiving stations, while customers can receive and send goods at the parcel-receiving stations. In addition, public air routes need to be planned between warehouses and stations to ensure the safety and efficiency of logistics UAV transportation. To sum up, the main research contents of this paper can be summarized as two points. One is the parcel-receiving station location problem on the land side, and the other is the public air-route planning problem on the air side.

The location method of the UAV parcel-receiving station can refer to the relevant research on UAV vertical airport (vertiport) locations. The main factors to be considered for vertiport locations include the construction cost [3,4], the coverage area [5], the storage capacity [6], and a special airspace environment with low-altitude transport characteristics [7,8]. However, the object of the above research is medium and large vertiports, which is different from the parcel-receiving station function studied in this paper. Similar research can also refer to the layout system of ground logistics facilities. Liu S et al. [9] studied the location of logistics pickup points, aiming to maximize the economic benefits of the transportation network, which is similar to the research scenario in this paper. There are also many types of research on the location problem of logistics pickup points, mainly considering the walking distance for customers to pick up goods, the coverage area of pickup points, etc. [10–12].

For UAV air-route planning, scholars in various countries mostly focus on the UAV path-planning field. Damilano et al. [13] emphasized that route creation is the core step of UAV task allocation and took the shortest time, minimum distance, minimum risk, etc., as the optimization goals of the UAV air route. Traditional methods to solve the problem of route planning mainly include fast search random tree [14], the artificial potential field method [15], genetic algorithms [16], ant colony algorithms [17], and the A* algorithm [18–20], among which the A* algorithm has an excellent route-planning ability in known environments. From the perspective of overall air-route configuration, Nanyang University of Technology [21] proposed three low-altitude route structures based on the urban layout, namely air matrix, over buildings, and over roads, and discussed the operation effects of three route configurations.

Although there have been some excellent research results in UAV vertiport location and public air-route planning, these studies are separated from each other and are two relatively independent research fields. Parcel-receiving stations and public air routes are both the basic guarantee facilities for UAV operation, and their layout should interact and influence each other. Therefore, a logistics UAV parcel-receiving station and public air-route planning method based on bi-layer optimization [22] is proposed in this paper, which determines the location scheme of the parcel-receiving stations and the layout structure of the public air-route at the same time. The output of the model meets the planning demands of both the landside and airside and supports the UAV logistics transportation mode of air–ground coordination.

2. Models

2.1. Problem Description and Model Assumptions

Due to the characteristics of high aggregation and strong repeatability of terminal demand points, it is difficult to directly use logistics UAVs for door-to-door distribution between the distribution warehouse and the demand points. In this paper, a UAV parcel-receiving station is set up in an area with intensive customer demand to receive and temporarily store logistics packages. The "last-mile" logistics transportation can be split into two parts: "distribution warehouse–parcel-receiving station" and "parcel-receiving station–demand point". Logistics UAV are used to perform the transportation task of "distribution warehouse–parcel-receiving station". Therefore, the problem solved in this paper can be described as follows: According to the location and demand volume of each demand point on the landside, reasonably locate the UAV parcel-receiving stations to obtain an economical, practical, and fair logistics UAV parcel-receiving station location scheme. Based on the location results, plan the public air-route configuration of logistics UAVs, and obtain a safe and efficient public air-route planning scheme for logistics UAVs.

To solve the transportation problem of "distribution warehouse–parcel-receiving station", the transportation network diagram $G = (N, E)$ can be defined, where $N = W \cup S$. N refers to the set of all nodes (UAV takeoff and landing points) in the transport network diagram, W refers to the set of distribution warehouses, S refers to the set of selected UAV parcel-receiving stations, and E refers to the set of connecting edges between nodes. The model proposed in this pater determines the layout scheme of the UAV parcel-receiving stations set S and designs the connection mode of the public air routes E simultaneously.

The assumptions of the logistics UAV parcel-receiving station and public air-route planning bi-layer optimization model are as follows:

1. The location of the distribution warehouse and the location and demand volume of each logistics demand point are known.
2. Take the multi-rotor UAV as the operating user, and the layered route strategy is adopted in air-route planning. The UAV can only adjust its flight altitude at the takeoff and landing area; the air routes with different operation directions are at different altitudes.
3. The distribution warehouse does not provide external services. Users can only pick up goods at the parcel-receiving station.
4. Due to the high accessibility and connectivity of ground-road junctions, all junctions are selected as alternative locations for parcel-receiving stations. Each alternative location is biased towards the open space beside the road to ensure that the construction of the parcel-receiving station does not affect the normal operation of ground traffic.

2.2. Operating Environment Modeling

Based on the model assumptions, the UAV only conducts climb and descent operations in its takeoff and landing area, and the remaining flight phases are conducted in a two-dimensional plane. Assume that the two-dimensional plane is a rectangle with length L and width W. The rectangle is divided into $u \times v$ grids with a square grid with grain size l_g, where $u = \mathrm{int}(Length/l_g)$, $v = \mathrm{int}(Width/l_g)$, and $\mathrm{int}()$ is the rounding function. The grid center point is the optional air-route point. When planning the air-route of logistics UAVs, the operational risks of UAVs should be considered comprehensively. UAV operational risks can be expressed as:

1. Collision risk

During actual operation, there is no-fly airspace for terrain obstacles such as tall buildings, which should be strictly avoided when planning logistics UAV air routes. To quantitatively describe airspace characteristics, grids in different special areas can be assigned different grid collision-risk values, as expressed in Table 1.

Table 1. Grid collision risk.

Grid Category	Flight Criteria	Collision Risk Value
No-fly airspace	no entry	1
dangerous airspace	flight allowed	D_g
free airspace	flight allowed	0

In Table 1, D_g is the collision-risk value of the dangerous airspace grid, which can be expressed as:

$$D_g = \frac{N_{obstacle(g)}}{N_{surround(g)}} \tag{1}$$

where $N_{obstacle(g)}$ refers to the number of no-fly airspace grids around grid g and $N_{surround(g)}$ refers to the total number of grids around grid g.

2. Crash risk

The crash risk can be defined by the "equivalent safety level" of the UAV, which is the number of casualties per unit of time:

$$S_g = P_{\mathrm{UAV}} \times E_g \times \left(1 - G_g\right) \times N_g \tag{2}$$

where S_g refers to the crash risk of the grid; P_{UAV} refers to the probability of UAV crash accident per hour—the current 5% NMAC standard is adopted in this paper, that is, the maximum collision probability between UAVs is 0.05; E_g refers to the ability of a UAV crash to cause damage, which is the sum of gravitational potential energy and dynamic potential energy of the UAV; N_g refers to the number of people affected in the grid, which is assumed to be one over land and zero over water for simplifying the model; and G_g refers to a safety barrier factor related to the geographical characteristics of the grid [23], with the specific settings shown in Table 2.

Table 2. Surface safety barrier factor.

Geographical Region	Safety Barrier Factor
open area	0
shrubbery	0.25
buildings below 20 m	0.5
buildings above 20 m	0.75

3. Noise risk

The UAV noise risk is mainly affected by three factors: noise source, noise barrier, and noise exposure. Noise source refers to the description of acoustic energy generated during UAV operation; noise barrier refers to the sound-blocking ability between the UAV and the noise-receiving object, which is approximate to the safety barrier factor; and noise exposure refers to the number of people affected by UAV noise. The noise risk is the additional noise perception under the normal operation background. This paper uses the residents' annoyance index to reflect the noise risk of UAV operation [24], which is expressed as:

$$L_g = N_g \times HA_g \times \left(1 - 0.08G_g\right) \tag{3}$$

where N_g refers to the number of people affected in the grid; G_g refers to the sound barrier factor, approximately the safety barrier factor; and HA_g refers to the residents' annoyance index, which is expressed as:

$$HA_g = \frac{123.81}{1 + \exp(9.99 - 0.15(L - \Delta L))} \tag{4}$$

where ΔL refers to the noise attenuation, which is related to the distance between the population and the air route in the grid:

$$\Delta L = 10 \cdot \lg\left(\frac{1}{4}\pi h^2\right) \tag{5}$$

where h refers to the vertical distance between the affected people and the air route.

The corresponding noise attenuation amounts of different floors are related to the number of floors and their height in the grid. For grids with multi-story buildings, the grid noise-risk index is the sum of the noise risk of all floors in the grid.

To avoid the magnitude difference between different operational risk values, we use the min–max standardization method for each UAV operational risk, which is expressed as:

$$A' = \frac{A - \min A}{\max A - \min A} \tag{6}$$

where $\min A$ and $\max A$ are, respectively, the minimum and maximum values of the risk indicators to be standardization.

2.3. Single-Air-Route Planning Model of Logistics UAV

In single-air-route planning, the objective is to ensure efficiency and safety, keeping the travel distance and flight risk of the UAV as low as possible. Based on the modeling results of the operating environment, the air route can be split according to the grids traversed when quantifying route costs. The set of grids through which the route passes can be stated as $G = \{g_i | i = 1, 2, \ldots, n\}$ of n grids. The travel distance of the UAV within the air route can be defined as the air range of the air route, reflecting the efficiency of the result. The flight risk of the UAV can be expressed as the product of the travel distance of the UAV in each spatial grid from G and the risk value of the grid, reflecting the safety of the result. Single-air-route planning is mainly limited by UAV performance, which is reflected in the setting of maximum air range and maximum turning angle of the air route.

The required parameters for the single-air-route planning mathematical formulation are presented in Table 3.

Table 3. Related parameters for single-air-route planning formulation defined.

Notations	
$AR_{\max}$	the maximum acceptable air range of the UAV air route
$\theta_{\max}$	the maximum acceptable turning angle of the UAV air route
Sets	
G	the set of grids through which the route passes
Variables	
n	the number of grids through which the route passes
(x_i, y_i)	the horizontal and vertical coordinates of grid i
D_i	collision-risk value of grid i
S_i	crash-risk value of grid i
L_i	noise-risk value of grid i
θ_i	turning angle of the air route at grid i

1. Objective function

Based on the parameters stated, the problem can be formulated as a minimization problem as

$$\min C_R = \sum_{i=1}^{n} (1 + D_i + S_i + L_i)\sqrt{(x_i - x_{i-1})^2 + (y_i - y_{i-1})^2} \tag{7}$$

Function (7) indicates that the single-route planning results should minimize the air range, collision risk, crash risk, and noise risk of the route.

2. Constraints

$$\sum_{i=1}^{n} \sqrt{(x_i - x_{i-1})^2 + (y_i - y_{i-1})^2} \le AR_{\max} \tag{8}$$

$$0 \le \theta_i = \arccos\left[\frac{(x_i - x_{i-1})(x_{i+1} - x_i) + (y_i - y_{i-1})(y_{i+1} - y_i)}{\sqrt{(x_i - x_{i-1})^2 + (y_i - y_{i-1})^2}\sqrt{(x_{i+1} - x_i)^2 + (y_{i+1} - y_i)^2}}\right] \le \theta_{\max} \tag{9}$$

Equation (8) refers to the maximum air-range constraint, indicating that the route air range should be less than the maximum travel distance of the UAVs. Equation (9) refers to the maximum turning-angle constraint, indicating that there should not be a turning angle exceeding the UAV's performance.

2.4. Parcel-Receiving Station and Public Air-Route Planning

The existing studies only focus on the problem of landing-point location or air-route planning. However, we believe that the location of parcel-receiving stations and the planning of public air routes are mutually influenced. In this section, the parcel-receiving station location problem and the public air-route planning problem are modeled as a bi-layer optimization problem. The upper-layer model is the parcel-receiving station location model, and the lower-layer model is the public air-route planning model. The public air-route planning needs to be based on the parcel-receiving station location results of the upper-layer model, and the evaluation criteria of the station location results is also affected by the public air-route planning results of the lower-layer model.

The upper-layer model is a multi-objective optimization model that is used to select a parcel-receiving stations set $S = \{s_i | i = 1, 2, \ldots, n_s\}$ of n_s stations from alternative locations. The objective of the upper-layer model is to minimize the selected station count, average picking distance, and picking distance standard deviation of unit demand in the planning area, so as to reflect the economy, practicability, and fairness of the location results. In order to meet the pick-up needs of all customers, each demand point in the demand point set $D = \{d_i | i = 1, 2, \ldots, n_d\}$ of n_d demand points should be assigned a parcel-receiving station. The customers of the demand point go to the assigned parcel-receiving station to receive and send parcels, which is called the matching relationship between demand point and parcel-receiving station.

The lower-layer model is a single-objective optimization model that is used to determine the configuration of the public air route. The public air route is the set of connecting edges $E = \{e_i | i = 1, 2, \ldots, n_s\}$ between the warehouse and the stations in a transport network diagram. The edge between two nodes is the output of the single air-route planning. The air route of parcel-receiving station s is a set $R_s = \{e_j | j = 1, 2, \ldots, n_r\}$ of the passing edges between the warehouse and the station in the public air route, where n_r refers to the number of passing edges. As in Section 2.3, in order to quantify the operating cost of public air routes, the edge e_i of set E can also be split according to the grids-traversed set $G^i = \left\{ g^i_j \middle| j = 1, 2, \ldots, n^i_e \right\}$ of n^i_e grids. The objective of the lower-layer model is to minimize the operating cost of the public air route, including the flight risk of the public air route and the air range of the air route between each warehouse and station, so as to reflect the safety and efficiency of the planning results.

Compared with the result of single-air-route planning, the air route of stations in the public air route includes a direct route and transit route to reduce the operating cost. The direct route is the same as the result of the single-route planning. The transit route can be represented as the UAV first flying to another station, and then flying from this station transit to the original station. As shown in Figure 1a, the black solid line is the single-air-route planning result between warehouse O and stations A, B, and C. In Figure 1b, the public air route contains three edges, namely OB, BA, and BC. The route OB is a direct route of station B, which is the same as the result of the single-route planning. The route OB–BA/BC is a transit route of station A/C. The UAV first flies over station B via edge OB and then transfers to BA/BC for station A/C. As can be seen, the overall length of the public air route is shorter and the potential risk to the operating area is less.

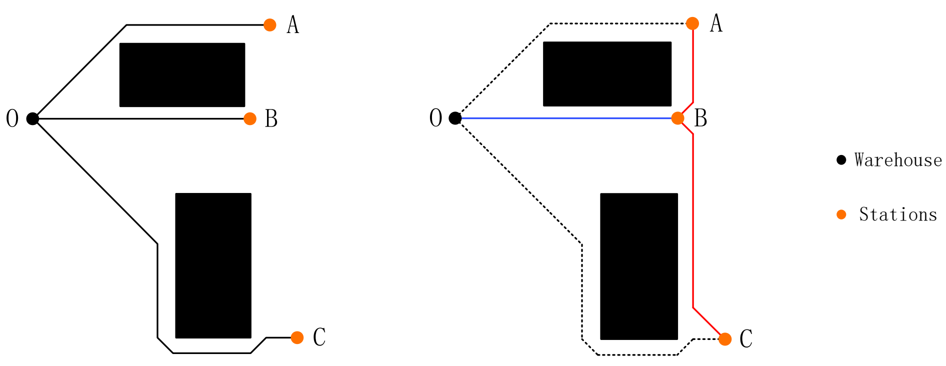

(**a**) (**b**)

Figure 1. Schematic diagram of air-route planning result. (**a**) Single-air-route planning result. (**b**) Public air-route planning result.

The new parameters for the parcel-receiving station and public air-route planning mathematical formulation are presented in Table 4.

Table 4. New parameters for parcel-receiving station and public air-route planning formulation defined.

Notations	
v_i	the demand volume of demand point i
$N_s^{\max}$	the maximum allowable number of parcel-receiving stations in the planning area
$d_{\max}$	the maximum acceptable picking distance for a customer
$C_{\min}$	the minimum capacity of parcel-receiving stations
$C_{\max}$	the maximum capacity of parcel-receiving stations
γ	the maximum acceptable negative air-range optimization rate
Sets	
S	the set of selected parcel-receiving stations
D	the set of demand points
E	the set of connecting edges between warehouse and stations
R_s	the set of edges through which the air route between warehouse and station s passes
G^i	the set of grids through which edge e_i passes
Variables	
x_{ij}	matching decision variable; equals 1 when the demand point i matches the parcel-receiving station j, otherwise 0
r_{kw}	edge-passing decision variable; equals 1 when the air route of station w passes edge k, otherwise 0
N_s	the number of selected parcel-receiving stations from alternative locations
n_e^k	the number of grids through which edge k passes
n_s	the number of grids through which the single air route of station s passes
d_i	the Manhattan distance from demand point i to its matching parcel-receiving station
d_{ij}	the Manhattan distance from demand point i to parcel-receiving station j
$\overline{d}$	the average Manhattan distance from unit demand to its matching parcel-receiving station
C_j	the service demand volume of parcel-receiving station j
$\lvert R_s \rvert$	the number of edges in the set R_s

2.4.1. Upper-Layer Model

1. Objective function

The upper-layer model of the logistics UAV parcel-receiving station location problem can be expressed as a multi-objective optimization problem as:

$$\min C_1 = N_s \tag{10}$$

$$\min C_2 = \frac{\sum\limits_{i \in D} v_i d_i}{\sum\limits_{i \in D} v_i} \tag{11}$$

$$\min C_3 = \frac{1}{\sum\limits_{i \in D} v_i} \sqrt{\sum_{i \in D} v_i \left(d_i - \overline{d}\right)^2} \tag{12}$$

Function (10) refers to the cost of selected parcel-receiving stations count, which reflects the economy of the location result. The smaller the result of Function (10), the fewer the number of the location result and the stronger the economy. Function (11) refers to the cost of the average picking distance, which reflects the practicality of the location result. The smaller the result of Function (11), the shorter the picking distance of unit demand and the stronger the practicability. Function (12) refers to the cost of picking fairness, which reflects the fairness of the location result. The smaller the result of Function (12), the smaller the picking distance gap per unit demand and the stronger the fairness.

2. Constraints

$$d_i = \min_{j \in S} d_{ij} \le d_{\max} \tag{13}$$

$$N_s \le N_s^{\max} \tag{14}$$

$$\sum_{i \in D} \sum_{j \in S} x_{ij} = 1 \tag{15}$$

$$C_{\min} \le C_j = \sum_{i \in D} v_i x_{ij} \le C_{\max} \tag{16}$$

Equation (13) indicates the maximum picking-distance constraint. Each demand point i of D should be matched to the nearest station j of S, and the picking distance between i and j cannot exceed the maximum acceptable picking distance $d$max. Since the ground roads are mostly square-format roads, Manhattan distance is used when calculating the picking distance. Equation (14) indicates the maximum selected parcel-receiving station count constraint; the number of parcel-receiving stations in the area cannot exceed the maximum allowable number $N_{\max}$. Equation (15) indicates the matching constraint; each demand point should match a parcel-receiving station. Equation (16) indicates the capacity constraint of the parcel-receiving station; the service demand of each parcel-receiving station must be within the specified range to avoid unnecessary parcel-receiving stations or exceeding the service capacity.

2.4.2. Lower-Layer Model

1. Objective function

The lower-layer model of the logistics UAV public air-route planning problem can be expressed as a minimization problem as:

$$\min C_4 = \sum_{k \in E} \sum_{v=1}^{n_e^k} \sqrt{(x_v - x_{v-1})^2 + (y_v - y_{v-1})^2} (D_v + S_v + L_v + \sum_{w \in S} r_{kw}) \tag{17}$$

Function (17) refers to the cost of public air-route operations, which reflects the safety and efficiency of the planning results, including the air range of the route between the warehouse and each station and the flight risk of the public air route.

2. Constraints

$$|R_s| \ge 1 \tag{18}$$

$$\sum_{k \in R_s} \sum_{v=1}^{n_e^k} \sqrt{(x_v - x_{v-1})^2 + (y_v - y_{v-1})^2} \le (1+\gamma) \sum_{v=1}^{n_s} \sqrt{(x_v - x_{v-1})^2 + (y_v - y_{v-1})^2} \tag{19}$$

$$\sum_{k \in R_s} \sum_{v=1}^{n_e^k} \sqrt{(x_v - x_{v-1})^2 + (y_v - y_{v-1})^2} \le AR_{\max} \tag{20}$$

Equation (18) is the route accessibility constraint. Each station can be reached by a set of edges in the public air route; that is, the number of edges in each route set R_s should not be less than 1. Equation (19) is the air-range negative optimization constraint; the route air range of each station in the public air route should be within an acceptable ratio compared to the air range of the single-air-route planning result. Taking Figure 1b as an example, assuming that the air range of OB–BA between O and A exceeds the acceptable ratio compared to the air range of OA, the transit route of OB–BA cannot be selected for the route of A when planning the public air route; instead, the direct route of OA should be selected. Equation (20) is the maximum air-range constraint, indicating that the route air range should be less than the maximum acceptable travel distance of the UAVs.

3. Algorithms

3.1. Single-Air-Route Planning Based on A Algorithm*

3.1.1. Valuation Function

1. Cost function

Based on the layered route strategy, it is assumed that the starting point S coordinate of the UAV is (X_0, Y_0) and the ending point E coordinate is (X_n, Y_n). The coordinates of a point P_x in the planned route are (X_x, Y_x), and the cost function is set according to Function (7) as follows:

$$g(x) = \sum_{i=1}^{x} (1 + D_i + S_i + L_i)\sqrt{(X_x - X_{x-1})^2 + (Y_x - Y_{x-1})^2} \tag{21}$$

2. Heuristic function

Euclidean distance is a widely used heuristic function form in the A* algorithm. We believe that UAV transportation should be mainly point-to-point flight, and only fly around in obstacle avoidance or high-risk areas. Therefore, using Euclidean distance as the heuristic function is suitable for the research scenario of this paper. The Euclidean distance between the current point P_x and the endpoint E can expressed as:

$$h(x) = \sqrt{(X_n - X_x)^2 + (Y_n - Y_x)^2} \tag{22}$$

The A* algorithm judges the merits and demerits of the track points through the valuation function $f(x)$, expressed as:

$$f(x) = g(x) + h(x) \tag{23}$$

3.1.2. Smooth Route

Due to the limitation of the path-finding direction of the A* algorithm in a two-dimensional grid environment, the air route can only be found in eight directions during air-route planning. Therefore, the planned UAV air route may have unnecessary turns due to the limitation of the air-route-finding direction of the A* algorithm, and such turns need to be smoothed. The smoothing idea is: For point P_i with a direction change in the planned air route, judge whether deleting P_{i+1} and connecting P_i directly with P_{i+2} will cause the air route to cross the no-fly airspace. If it does not cross the no-fly airspace and segments P_i–P_{i+2} meet the constraints of route planning and the total cost is smaller, then delete route point P_{i+1} and update segments P_i–P_{i+1}–P_{i+2} to P_i–P_{i+2}. Repeat this operation until there is no change in each segment of the output route. As shown in Figure 2, the initial air-route segment is P_1–P_2–P_3–P_4–P_5–P_6–P_7–P_8, which is updated to P_1–P_8 after smoothing.

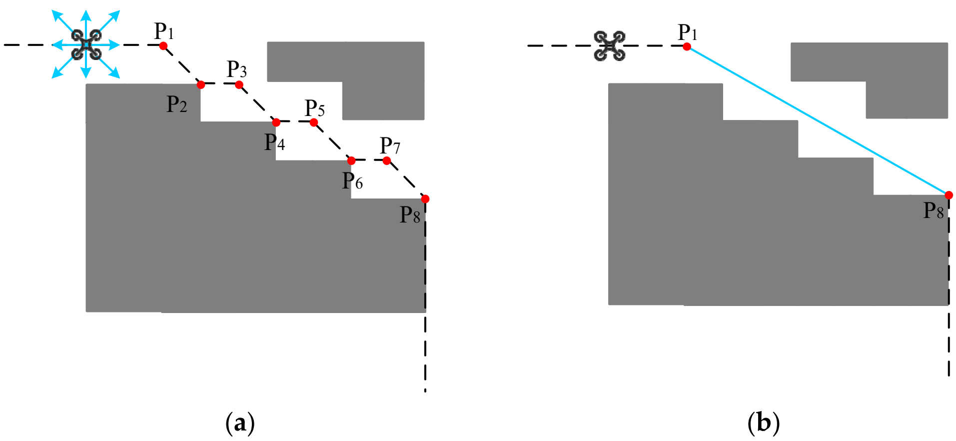

Figure 2. Air-route smoothing result. (**a**) Before smoothing. (**b**) After smoothing.

3.1.3. Single-Air-Route Planning Flow

The processes of single-air-route planning can be described as follows:

Step 1: Obtain the starting point S and ending point E, establish the OPEN and CLOSE list, and add the starting point S to the OPEN list.

Step 2: Judge whether the OPEN list is empty. If it is not empty, perform the following steps; otherwise, turn to Step 7.

Step 3: Pop up the grid point with the smallest $f(x)$ value in the OPEN list, take this grid point P as the next air-route point, and put it in the CLOSE list.

Step 4: Judge whether point P is the ending point. If it is the ending point, turn to step 7; otherwise, turn to step 5.

Step 5: Check the grid points adjacent to point P. If the adjacent grid points are not in the OPEN list, add them to the OPEN list, and take point P as the parent node of the new grid. If the adjacent grid points are in the OPEN list, check whether the cost of the current path is minimum.

Step 6: Recalculate $g(x)$, $h(x)$, and $f(x)$ according to the cost function, and return to step 3.

Step 7: Judge whether the ending point E is reached. If the endpoint has been reached, turn to Step 8; otherwise, the planning fails.

Step 8: Smooth the air-route planning result and output the air route.

3.2. Parcel-Receiving Station and Public Route Planning Based on GA-MMAS

In this section, the genetic algorithm (GA) is used to solve the upper-layer model of the logistics UAV parcel-receiving station location problem and determine the layout of the parcel-receiving station from alternative locations. Then, based on the current location scheme, determine the public air-route structure using the max–min ant system (MMAS). Use the GA-MMAS algorithm for nesting optimization to obtain the logistics UAV parcel-receiving station and public air-route planning results.

3.2.1. Parcel-Receiving Station Location Based on GA

1. Population initialization

   (1) Chromosome coding

The logistics UAV parcel-receiving station location model is a 0–1 integer programming model. Randomly assign 0–1 variables to the alternative location of the parcel-receiving station during chromosome coding. Zero means no parcel-receiving station is set at this alternative location, and one means a parcel-receiving station is set at this alternative location, as shown in Figure 3:

0	1	1	0	0	0	1	1	0	0

Figure 3. Chromosome coding mode.

   (2) Initial population generation

According to the chromosome coding mode, N^{U} initial individuals are randomly generated to obtain the initial population.

2. Fitness calculation

Individual fitness is an indicator to measure the degree of individual excellence. In this section, individuals are ranked according to their performance to determine the fitness of each individual. For each cost i, generate a sequence X_i based on the performance of each individual to the cost, and the fitness of the individual to the cost is reflected by the order of individuals in the sequence. The fitness calculation formula of individual j to cost i is as follows:

$$F_j(X_i) = \begin{cases} (N^{\mathrm{U}} - (R_j(X_i))^2, R_j(X_i) > 1 \\ k(N^{\mathrm{U}})^2, R_j(X_i) = 1 \end{cases} \tag{24}$$

where $F_j(X_i)$ refers to the fitness of individual j to cost i; N^{U} refers to the total population; $R_j(X_i)$ refers to the sequence number of individual j in sequence X_i after all individuals in the population rank the cost i; and k is a constant in the interval [1,2] that can increase the fitness of the best individual with a single objective.

According to the optimization objective, the overall fitness of the individual population is:

$$F(X_j) = \sum_{i=1}^{n} \omega_i F_i(X_j) \tag{25}$$

where $\sum_{i=1}^{n} \omega_i = 1$; n refers to the number of costs to calculate.

3. Genetic operator operation

(1) Select

Ranking-based selection is used in this section. The individuals in the population are sorted from the best to the worst, and the parent individuals are selected by ranking and roulette. We use ranking-based selection instead of the absolute fitness value to prevent premature convergence of the algorithm.

(2) Crossing and mutation operators

In order to avoid overmodifying the original solution and the potentially superior solution, double-point crossover and 0–1 single-mutation change are used. Double-point crossover refers to selecting two cross nodes and exchanging the sequence between the corresponding nodes in two-parent individuals. A 0–1 single-mutation change refers to modifying the 0–1 variable at a certain position of an individual chromosome. The crossing and mutation operators are shown in Figures 4 and 5.

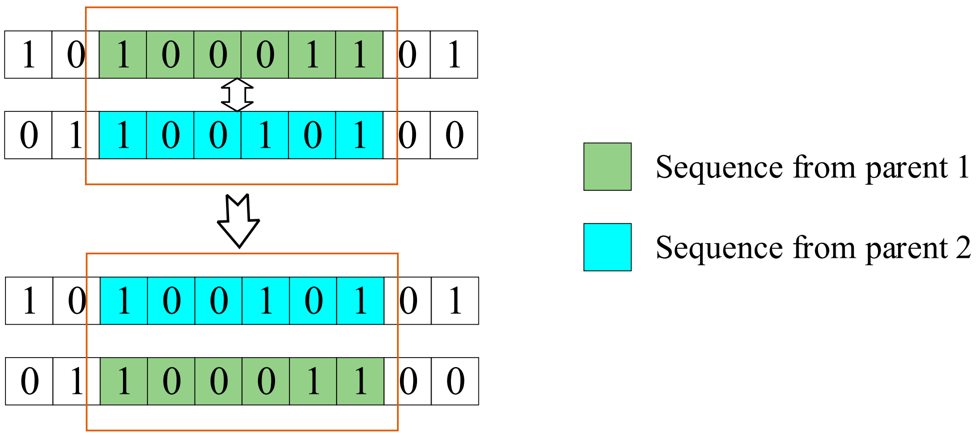

Figure 4. Schematic diagram of double-point crossover.

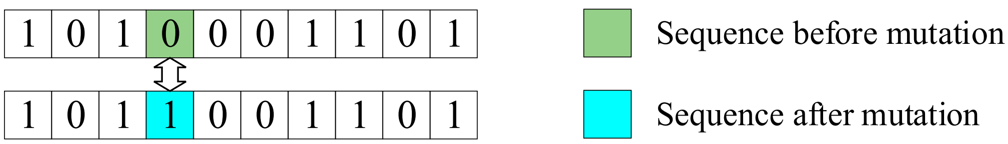

Figure 5. Schematic diagram of 0–1 single mutation.

(3) Genetic parameter adaptation

The main factors affecting the behavior of the genetic algorithm include the crossing probability P_c and mutation probability P_m. The choice of crossing probability P_c and mutation probability P_m will affect the convergence of the algorithm. In this section, the genetic parameters are adaptively adjusted. The adjustment formula is as follows:

$$P_c = \begin{cases} P_{c1} - \frac{(P_{c1}-P_{c2})(A'-A_{avg})}{A_{\max}-A_{avg}}, A' \geq A_{avg} \\ P_{c1}, A' < A_{avg} \end{cases} \tag{26}$$

$$P_m = \begin{cases} P_{m1} - \frac{(P_{m1}-P_{m2})(A_{\max}-A)}{A_{\max}-A_{avg}}, A \geq A_{avg} \\ P_{m1}, A < A_{avg} \end{cases} \tag{27}$$

where A' refers to the higher fitness among the two individuals who perform crossover operators, A refers to the fitness of individuals undergoing mutation, $A_{\max}$ refers to the maximum fitness in the population, and A_{avg} refers to the average fitness in the population. To reduce the probability of mutation and crossing of individuals with excellent performance, we make individuals with a relatively poor performance have a higher probability of variation. Generally, $P_{c1} = 0.9, P_{c2} = 0.6, P_{m1} = 0.1, P_{m2} = 0.001$ [25].

3.2.2. Public Air-Route Planning Based on MMAS

The process of determining the public air-route configuration is the process of generating the minimum tree for all nodes. The greedy algorithm is used when planning the route of each station with a certain planning sequence to form the public air route. When planning the route for station i, based on the public air-route planning results of the first i-1 stations, we select the node-connection mode with the smallest increment to Function (17). According to Function (17), if the route of station i is a direct route, Function (17) should increase the air-range cost and flight-risk cost of the direct route on the basis of its original value. If the route of station i is a transit route, Function (17) should increase the cost of the air range passed by all edges and the cost of the flight risk from the transit point to station i on the basis of its original value. As shown in Figure 6a, the dotted line in Step 0 is the set of edges that can be selected between nodes after single-air-route planning. In Step 0, since there is no station that has a planned route with warehouse O, only the direct route OA can be planned for station A. In Step 1, because there is an air route between stations A and O, we can choose to plan the OC direct route and OA–AC transit route when planning the air route for station C. According to Function (17), the increased cost of the OC direct route includes the air-range cost and flight-risk cost of edge OC. The increased cost of the OA–AC transit route includes the cost of the air range of edge OA and edge AC and the cost of the flight risk of edge AC. We compare the increased cost of OC and OA–AC and choose the smaller increased cost-planning method (in Figure 6a, it is assumed that the increased cost of OC is smaller). In Step 2, the route that can be planned for station B includes the direct route OB and the transit routes OA–AB and OC–CB, and the planning method with the minimum increased cost is selected (OA–AB is assumed to have the minimum increased cost in the figure). In the order of the planning sequence of A–C–B, the route of station A is the direct route OA, the route of station B is the transit route OA–AB, and the route of station C is the direct route OC. The public air-route contains three edges, which are OA, AB, and OC.

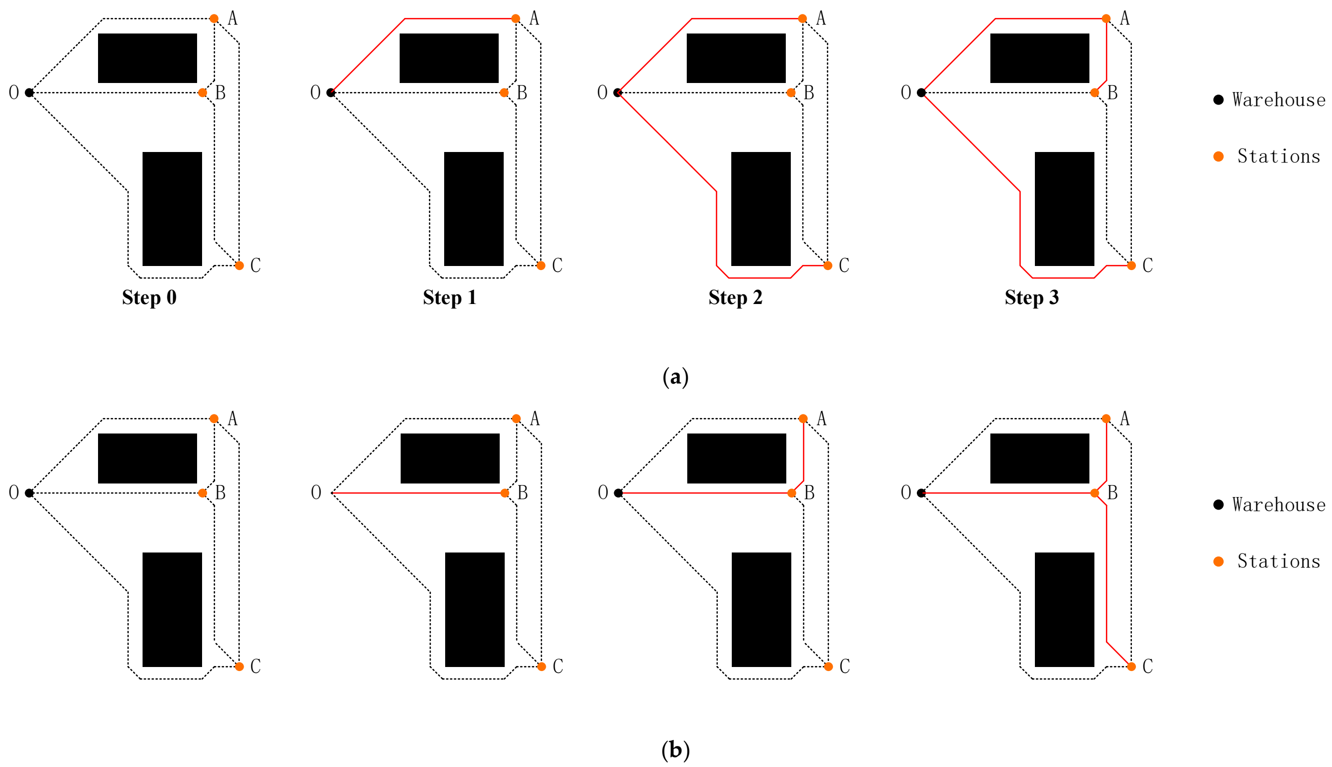

Figure 6. Public air-route planning process. (**a**) Public air-route planning sequence of A–C–B. (**b**) Public air-route planning sequence of B–A–C.

In Figure 6b, we find that different route configurations can be obtained with the planning sequence of B–A–C using the same greedy algorithm. The route of station A is the transit route OB–BA, the route of station B is the direct route OB, and the route of station C is the transit route OB–BC. The public air-route contains three edges, which are OB, BA, and BC. Therefore, after the parcel-receiving station location is determined, it is also necessary to determine the optimal public air-route planning sequence of stations, and then plan the public route according to the greedy algorithm above to obtain the optimal public route configuration.

In this section, the max–min ant system (MMAS) is used to solve the route-planning sequence of each parcel-receiving station and then determine the configuration of the public air route. Compared with the ordinary ant colony algorithm, the max–min ant system used in this section is mainly different in the following ways:

1. The max–min ant system strengthens the feedback of the optimal path information, only allowing the pheromone updates on the optimal path of each generation:

$$\tau_{ij}(t+1) = (1-\rho)\tau_{ij}(t) + \Delta\tau_{ij}^{best} \tag{28}$$

   where $\Delta\tau_{ij}^{best} = 1/c_{best}$, and c_{best} refers to the optimal ant's total cost of public air-route operating in this iteration. The cost of each ant can be calculate by Function (17).

2. To prevent the algorithm from falling prematurely, pheromones of each path are determined in the interval $[\tau_{\min}, \tau_{\max}]$, where:

$$\tau_{\max} = \frac{1}{1-\rho}\frac{1}{c_{best}} \tag{29}$$

$$\tau_{\min} = \frac{2\tau_{\max}(1-\sqrt[n]{p_{best}}}{(n-2)\sqrt[n]{p_{best}}}\frac{1}{c_{best}} \tag{30}$$

where p_{best} refers to the probability of ants finding the shortest path in one exploration. The max–min ant system efficiency is not sensitive to the value of p_{best}, which is generally 0.05 [26].

3. Unlike the basic ant algorithm, which initializes the pheromone to a minimum value, the max–min ant system initializes the pheromone to a maximum value $\tau_{\max}$.

In addition, to avoid unnecessary calculations, an early-stop condition is set for MMAS. MMAS can be stopped in advance when the optimal results of successive N_{ES}^{MMAS} generations do not change.

3.2.3. Parcel-Receiving Station and Public Air-Route Planning Strategy

In this paper, the genetic algorithm and max–min ant system are nested to solve the logistics UAV parcel-receiving station and public air-route planning problem. First, the genetic algorithm is used to generate the location scheme, and the max–min ant system is used to carry out the public route-air planning for each location scheme in the population. The comprehensive fitness of each individual in the population to each cost is calculated and genetic operators such as crossing and mutation operators are performed on the population. We then iterate through the above operations until the end of the algorithm.

This nested solution of GA-MMAS requires a great deal of computational power. When MMAS is used to solve the lower-layer model, the calculation amount of the route-planning sequence with the minimum public air-route operating cost is positively correlated with the number of stations to be planned. In addition, when the number of station location results is too large, the selected stations count cost of the upper-layer model is higher and the economy of the location scheme is poor, so this kind of solution is not the best solution to this problem. Therefore, to reduce the calculation amount and improve the calculation efficiency, the genetic algorithm can be used to solve only the upper-layer model and obtain the parcel-receiving station location scheme without considering the influence of the lower-layer model. When performing the GA-MMAS algorithm nesting solution, the number of parcel-receiving stations N_S is scaled. If the number of parcel-receiving stations N_i is greater than $(1+\chi)N_S$, it will not be transferred to the calculation of public air-route planning to avoid unnecessary waste of computing resources.

3.2.4. Parcel-Receiving Station and Public Air-Route Planning Flow

The pseudo-code and algorithm flow chart of the GA-MMAS is shown in Algorithm 1 and Figure 7. In the solution, the cost of the selected station count, the cost of the average picking distance, the cost of picking fairness, and the cost of public air-route operation are considered. If the number of parcel-receiving stations in the parcel-receiving station location scheme exceeds $(1+\chi)N_S$, it will not be transferred to the lower-layer model for the solution, making the cost of public air-route operation infinite. Otherwise, we use the max–min ant system to calculate the public air-route operating cost, and the individual fitness of the parcel-receiving station and public air-route planning scheme is calculated based on the cost sequence with Function (24). The upper-layer model fitness F_i^{U} of scheme i includes the cost of the selected station count F_{i1}, the cost of the average picking distance F_{i2}, and the cost of picking fairness F_{i3}, expressed as $F_i^{\mathrm{U}} = \omega_1 F_{i1} + \omega_2 F_{i2} + \omega_3 F_{i3}$, where $\omega_1 + \omega_2 + \omega_3 = 1$. The total fitness F_i is the sum of the fitness of the parcel-receiving station location results and the public air-route planning results, expressed as $F_i = \phi_1 F_i^{\mathrm{U}} + \phi_2 F_i^{\mathrm{L}}$, where $\phi_1 + \phi_2 = 1$.

Algorithm 1 The GA-MMAS pseudo-code.

```
GA_iter = 0;//Iteration times of GA
Parents = InitializeP(N^U);//Initialize population with scale N^U
While(GA_iter < max_GA_iter){
    for i = (1:N^U){
        c_num[i], c_dis[i], c_fair[i] = cal_cost(P[i]);//calculate station count cost, distance cost, and fair cost
        if (c_num[i] < upper_num){c_route[i] = MMAS(P[i]);}
        else{c_route[i] = inf;}
        }
    Fitness = cal_FitnessP(c_num, c_dis, c_fair, c_route);
    Children = GA-OperationP(Parents, Fitness);//GA operations such as crossing and mutation
    P = Children;
}
```

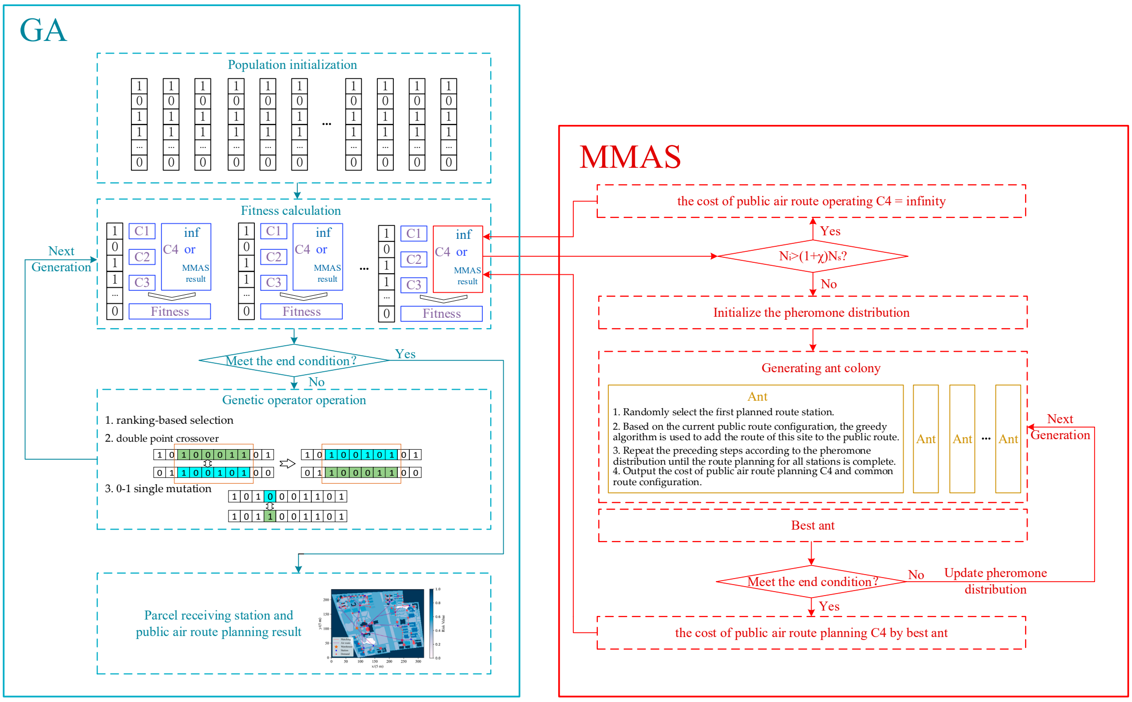

Figure 7. GA-MMAS algorithm flow chart.

The max–min ant system pseudo-code of the public air-route planning model is shown in Algorithm 2. Based on the pheromone distribution and greedy algorithm, the optimal public air-route planning sequence, optimal public air-route configuration, and minimum public air-route operating cost were obtained.

Algorithm 2 The max–min ant system pseudo-code.

```
init antCount, alpha, beta, and other coef's
for j = (1:max_MMAS_iter){
    for k(1:antCount){lower_cost[j][k] = cal_route_cost(pheromone);}
    c_route[i] = min(lower_cost[j]);
    pheromone = update(min(lower_cost[j]));//updating pheromone matrix using the best ant}
    }
Output(min(lower_cost[j]));
```

4. Simulation and Analysis

4.1. Simulation Environment

In this paper, the Jiangjun Road Campus of Nanjing University of Aeronautics and Astronautics is selected as the simulation scene. The selected scene is rasterized, and the collision-risk, crash-risk, and noise-risk values of each grid are calculated. The grid attribute map is shown in Figure 8:

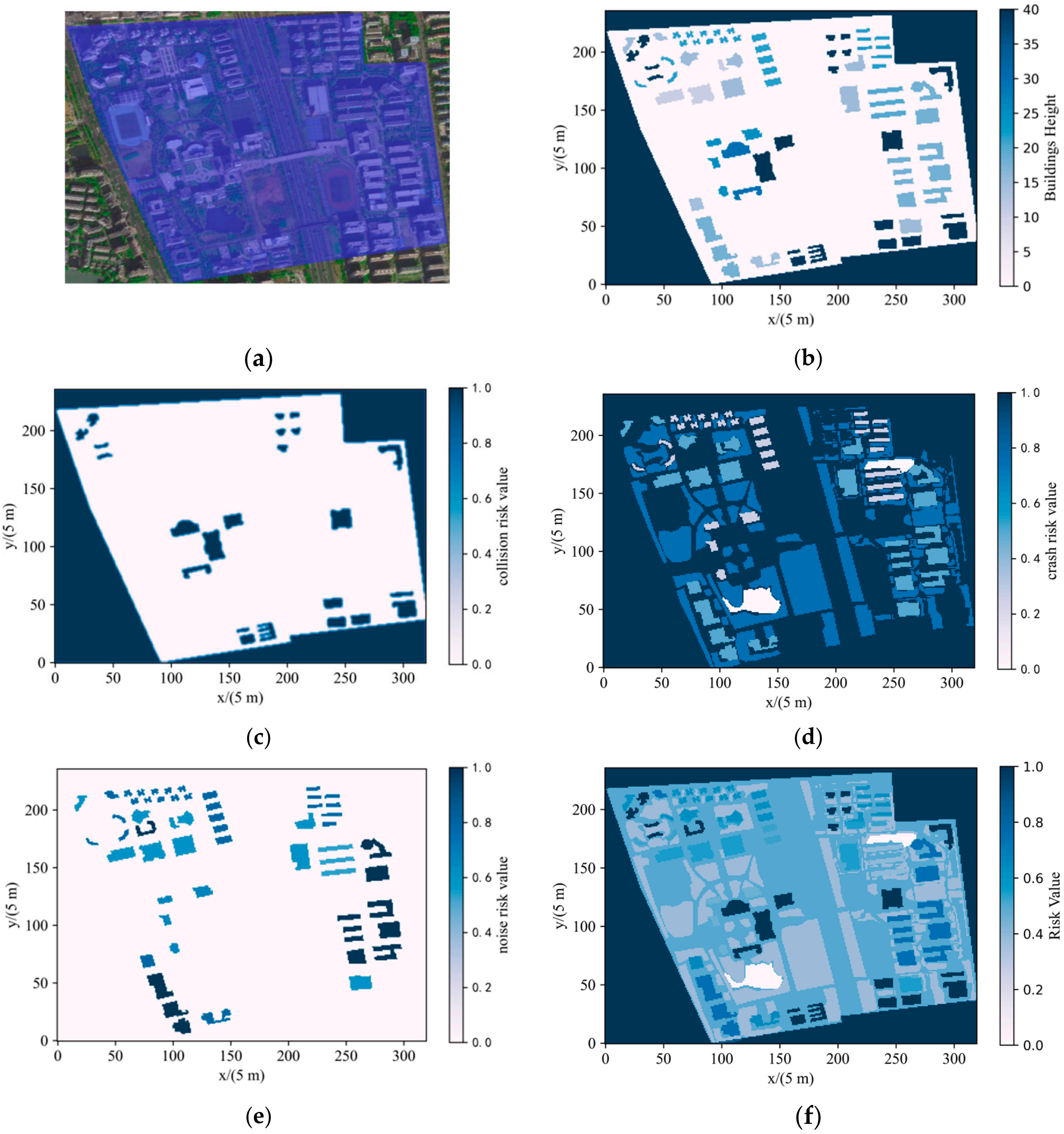

Figure 8. Grid attribute map. (**a**) Real map of the simulation scene. (**b**) Obstacle height map. (**c**) Grid collision-risk value. (**d**) Grid crash-risk value. (**e**) Grid noise-risk value. (**f**) Grid comprehensive risk value.

The demand distribution can be calculated from the number of grids and floors occupied by each building, and the entrance of each building is selected as the demand point distribution location, as shown in Figure 9 and Table 5. The open space beside the ground-road junctions in the simulation scenario is selected as the alternative location of the parcel-receiving station. See Figure 10 for the distribution of the 122 alternative locations of the parcel-receiving station.

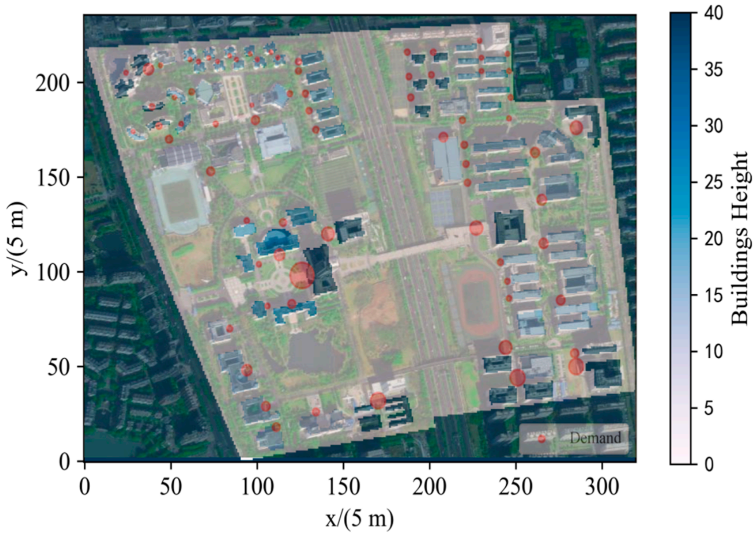

Figure 9. Distribution of logistics demand.

Table 5. Distribution and volume of logistics demand.

Demand Volume	The Number of Demand Point	Proportion/%
(0,200]	12	16.22
(200,500]	36	48.65
(500,1000]	12	16.22
(1000,5000]	13	17.56
>5000	1	1.35
total number	74	
total volume	55,787	
minimum volume	132	
maximum volume	7546	
average volume	754	

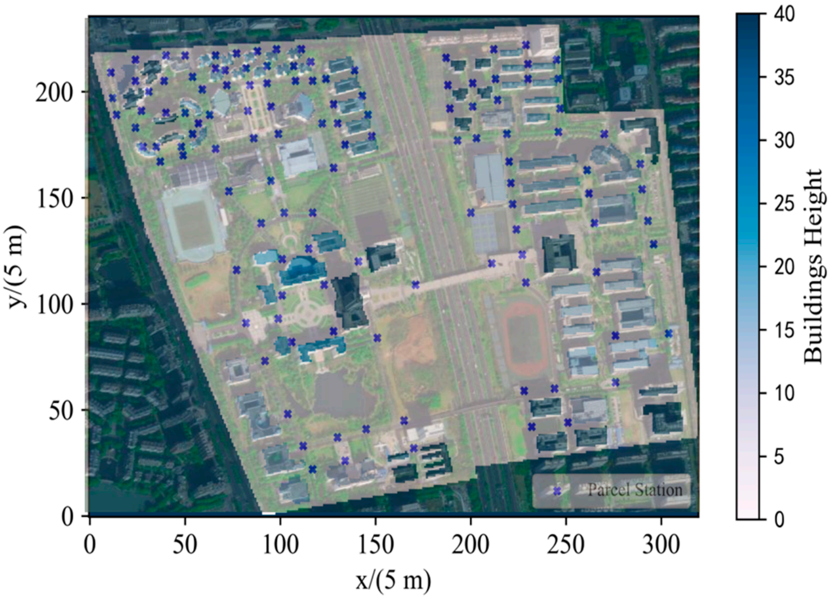

Figure 10. Alternative locations of the package-receiving station.

After airspace rasterization, 320 × 236 airspace grid matrices can be obtained. The height of the building grid is mainly 15–30 m. In order to facilitate supervision and reduce the impact on ground activities, we plan distribution routes with the same structure and different levels for UAV round-trip distribution. In the simulation, it is assumed that the round-trip routes are arranged at 30 m and 50 m [26], and the operational risk is considered when the UAV flies at 40 m. The settings of other simulation parameters are shown in Table 6 [8,27,28].

Table 6. Simulation parameter settings.

Parameter	Value	Parameter	Value
Maximum UAV air range $L_{\max}$/m	3000	Minimum cost-scaling factor k	1.5
Maximum UAV turning angle $\theta_{\max}$	$\pi/2$	Upper-layer model fitness weight φ_1	0.5
Maximum negative route optimization γ	20%	Lower-layer model fitness weight φ_2	0.5
Maximum acceptable picking distance $d_{\max}$/m	200	Parcel-receiving station count weight ω_1	0.6
Grid width/m	5	Average picking distance weight ω_2	0.2
Maximum picking distance point $d_{\max}$/m	200	Picking fairness weight ω_3	0.2
Maximum parcel-receiving station count $N_s^{\max}$	74	Pheromone volatilization factor ρ	0.95
Maximum parcel-receiving station capacity $C_{\max}$	15,000	Pheromone factor α	1.0
Minimum parcel-receiving station capacity $C_{\min}$	1000	Heuristics factor β	1.0
GA population size N^U	50	Ant colony size m	50
GA maximum iterations $N_{\max}^{\mathrm{GA}}$	200	MMAS maximum iterations $N_{\max}^{\mathrm{MMAS}}$	200
Parcel-receiving station scaling χ	0.5	MMAS early-stop iteration N_{ES}^{MMAS}	20

4.2. Results of Analysis

According to the above simulation scenarios and simulation data, the logistics UAV parcel-receiving station and public air-route planning model is solved. All experiments were performed on a server with 4.7 GHz Intel-Core i7 processors, 16 GB RAM, with Windows Server 11 Operating System and the maximum solution time set to 3600 s. We repeated the experiment for 30 groups. The average solution time was 2352 s, and we selected one group to display the best solution.

The solution results of the bi-layer model are shown in Figure 11, and Tables 7 and 8. The number of parcel-receiving station locations is 17, the average picking distance is 98.10 m, and the picking distance standard deviation of unit demand is 49.22 m. Each parcel-receiving station matched two to ten demand points. Among them, 12 package-receiving stations have matching demand between 2000 and 5000. There are three parcel-receiving stations with a demand of less than 2000 and one parcel-receiving station with a demand of more than 10,000. The public air routes include 17 edges, forming 17 routes connecting the warehouse and stations, including four direct routes and 13 transit routes. After optimization, the air route between any two points is an almost straight line between two points, and some routes have a small amount of bends due to obstacle avoidance or high comprehensive risk.

Table 7. Location results of parcel-receiving stations.

Station Number	Demand Point	Demand Volume	Station Coordinates	Station Number	Demand Point	Demand Volume	Station Coordinates
1	6	2052	(28, 174)	10	5	2886	(221, 157)
2	10	3121	(66, 211)	11	3	2943	(229, 110)
3	8	2334	(116, 214)	12	2	2320	(266, 115)
4	5	2154	(99, 180)	13	4	3568	(270, 180)
5	2	1125	(95, 158)	14	5	2046	(201, 193)
6	4	11668	(123, 109)	15	5	1140	(230, 213)
7	4	1807	(106, 82)	16	3	5309	(244, 60)
8	2	3561	(145, 41)	17	3	4703	(276, 63)
9	3	3050	(112, 33)				

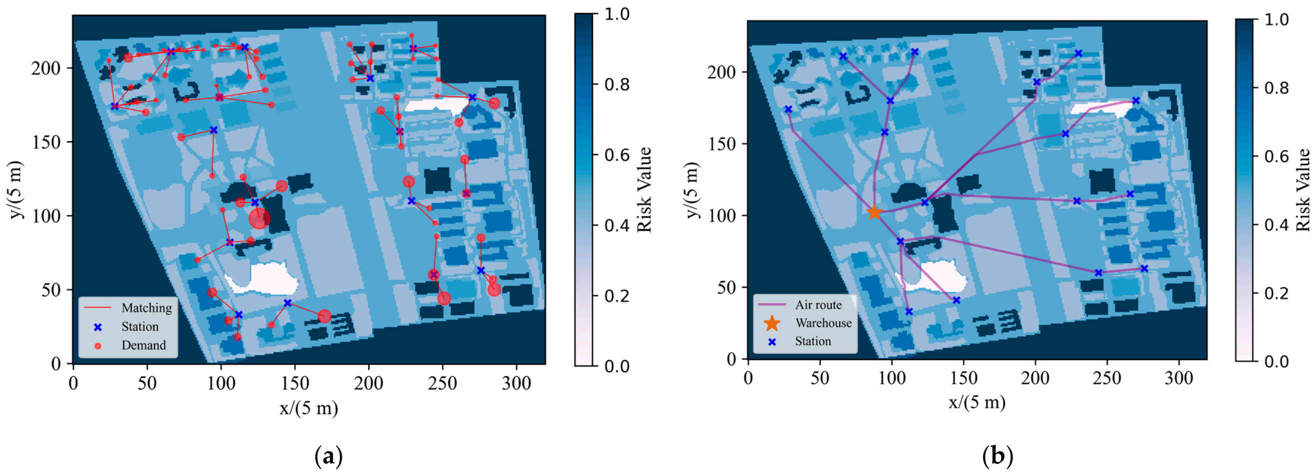

Figure 11. Logistics UAV parcel-receiving stations and public air-route planning result. (**a**) Parcel-receiving station location results and demand-point-matching relationship. (**b**) Public air-route planning results based on MMAS.

Table 8. Public air-route planning results.

		Direct Air Route	Public Air Route	Optimization Rate	Passing Station
air-range cost	route1	93.72	93.72	0.00%	1
	route2	111.38	124.47	−11.75%	5, 4, 2
	route3	115.45	117.21	−1.52%	5, 4, 3
	route4	79.20	79.19	0.01%	5, 4
	route5	56.83	56.83	0.00%	5
	route6	35.69	35.69	0.00%	6
	route7	26.91	26.91	0.00%	7
	route8	85.25	84.18	1.25%	7, 8
	route9	74.78	76.62	−2.46%	7, 9
	route10	149.81	148.57	0.83%	6, 10
	route11	142.84	143.48	−0.45%	6, 11
	route12	179.98	181.10	−0.62%	6, 11, 12
	route13	206.26	205.17	0.52%	6, 10, 13
	route14	150.09	153.15	−2.04%	6, 14
	route15	186.52	189.09	−1.38%	6, 14, 15
	route16	162.75	167.90	−3.16%	7, 16
	route17	194.10	200.04	−3.06%	7, 16, 17
collision risk		4.40	2.82	35.81%	
crash risk		487.92	263.73	45.95%	
noise risk		112.08	76.16	32.05%	
total risk		604.40	342.72	43.30%	
total cost		2558.40	2426.04	5.17%	

Compared with the public air route combined with the direct route (the results of the single-air-route planning) for all stations, the total risk is significantly reduced by 43.30%, and the cost of public air-route operation is reduced by 5.17%. This result proves the effectiveness of using MMAS to solve the lower-layer model, and a public air-route planning scheme with a lower cost is obtained using MMAS under the same location-selection results. According to the analysis of each air route, nine of the 17 routes had a negative optimization of the route's air range, of which eight routes had a negative optimization rate of less than 5% and one route had a negative optimization rate of 10–15%. In addition, there are four air-range-optimization routes among the 13 transit routes. Analyzing the results, the planned route of the A* algorithm is not the optimal solution, and the route-smoothing method used in this paper cannot ensure that the route can be smoothed into the optimal configuration, which further increases the uncertainty of the route cost. Therefore, some transit routes composed of multiple edges may have slightly better planning results than direct routes, which is caused by the limitations of A* algorithm and the smoothing method used in this paper. The optimization degree of the four distance-optimization routes is not high, namely, 0.01%, 0.52%, 0.83%, and 1.25%, respectively. This also proves that although the single-air-route planning method proposed in this paper has some volatility, its overall results are excellent. Otherwise, compared with the public air route combined with the direct route for all stations in Figure 12, the route configuration in Figure 11 is simpler, the number of intersections is less, and it is easier to supervise the UAV operation.

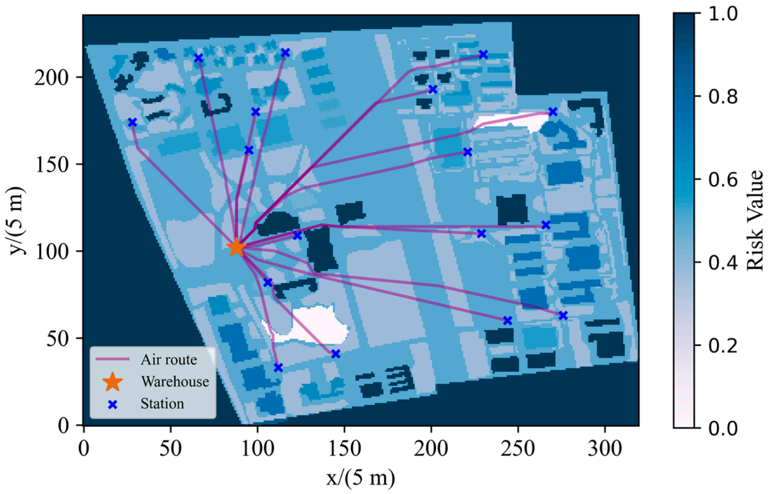

Figure 12. Public air route combined with the direct route for all stations.

The actual layout of round-trip public air routes is shown in Figure 13. In the figure, the blue route is the public route for delivery, the red route is the public route for returning, and the blue column is the vertical takeoff and landing procedure of the UAV at the distribution warehouse and parcel-receiving station. In actual operation, the logistics UAV starts from the distribution warehouse, climbs to the height of the delivery route according to the established vertical takeoff and landing procedure, uses the delivery route to transport the logistics parcels to the parcel-receiving station, places the parcels according to the takeoff and landing procedure, climbs to the height of the return route, and returns to the distribution warehouse using the return route with an empty aircraft.

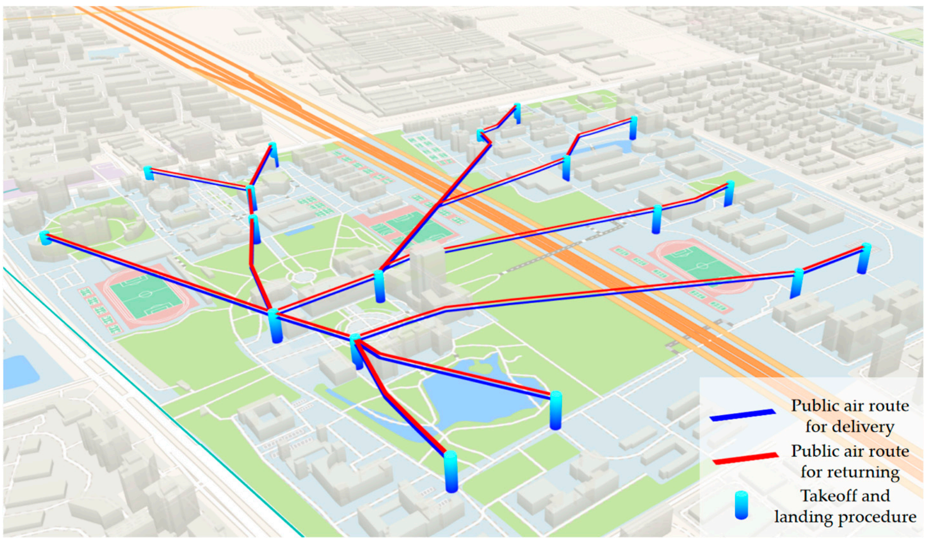

Figure 13. The actual layout of round-trip public air routes.

4.3. Parameter-Setting Analysis

In this section, we study the influence of different weight settings on the model output results. We set ω_1, ω_2, ω_3 and took 0.1 as the step size, then set 36 groups of control tests, where $\omega_1 + \omega_2 + \omega_3 = 1$. The experiment was repeated 30 times in each group, and the results were averaged. The costs of the upper-layer model vary with the weight as shown in Figure 14. It can be observed that each cost has different sensitivities to different weights, and there is no single right reorganization. The Pareto optimal solution of each weight-recombination category is selected as shown in Table 9, which can be roughly divided into two categories. The first five groups, that is, when $\omega_1 \leq 0.4$, tend to exchange a higher selected station count for a lower average picking distance and a lower picking distance difference of unit demand. The last five groups, that is, when $\omega_1 \geq 0.5$, tend to exchange a higher average picking distance and picking distance difference for a lower selected station count. On the one hand, according to the optimization objective Function (17), it can be seen that the lower-layer model tends to have a better performance in the location scheme with a lower station count. Therefore, after the inclusion of the lower model, the algorithm may be more inclined to choose the scheme with a smaller station count. On the other hand, a high selected station count is not conducive to the quick solution of the lower-layer model, and the specific analysis will be given in Section 4.4. Therefore, among the five solutions of $\omega_1 \geq 0.5$, weight group 8 (0.6, 0.2, 0.2) with the most balanced performance among the three costs of the upper-layer model is selected as the weight combination of the upper-layer model.

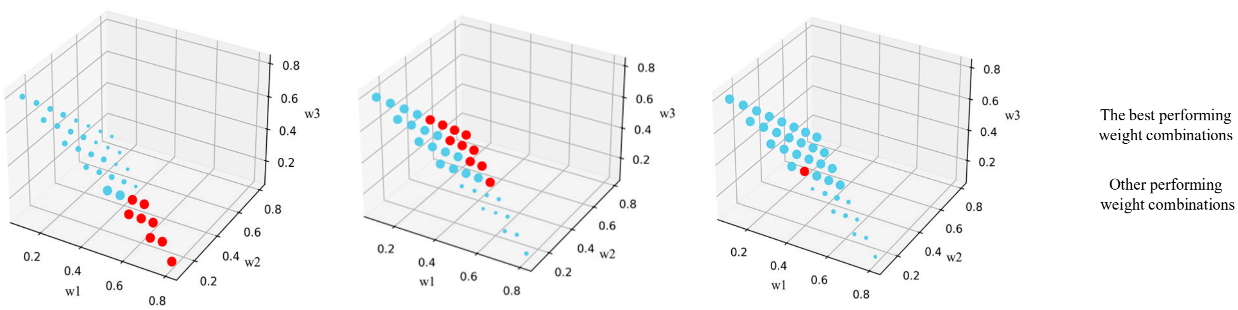

(**a**) (**b**) (**c**)

Figure 14. Cost of different upper-layer model-weight combinations. (**a**) Selected parcel-receiving station count. (**b**) Average picking distance. (**c**) Picking fairness.

Table 9. Pareto optimal solution with different weight combinations.

Group	Weight Scale	Parcel-Receiving Station Count	Average Picking Distance	Standard Deviation of Picking Distance
1	0.1, 0.6, 0.3	62.0	31.08	36.87
2	0.3, 0.4, 0.3	50.8	34.67	36.29
3	0.4, 0.1, 0.5	52.0	35.00	36.17
4	0.4, 0.2, 0.4	52.0	35.14	36.14
5	0.4, 0.4, 0.2	55.0	33.29	36.52
6	0.5, 0.2, 0.3	17.5	108.00	59.81
7	0.5, 0.3, 0.2	17.0	108.02	57.31
8	0.6, 0.2, 0.2	17.0	100.78	61.32
9	0.6, 0.3, 0.1	17.0	97.42	63.38
10	0.8, 0.1, 0.1	17.0	97.03	64.26

Further study of the weight proportion of the upper-layer model and the lower-layer model after determining the weight proportion of the three costs of upper-layer model was conducted. We set φ_1 and φ_2, took 0.1 as the step size, and set nine groups of control tests, where $\phi_1 + \phi_2 = 1$. The experiment was repeated 30 times in each group, and the results were averaged. Based on the layered solution results of the parcel-receiving station location and the public air-route planning, the cost changes of each weight combination are shown in Table 10. It is observed that there is no obvious change trend among the weight combinations, but the cost of public air-route operation of each weight combination is better than those of the layered solution results. After adding the lower-layer model, the public route planning affects the location scheme of the upper-layer model. The average selected station count increased, which also resulted in a decrease in the average picking distance and picking distance variance. It can be seen that the upper-layer model of parcel-receiving station location and the lower-layer model of public air-route planning influence each other, and the bi-layer optimization model proposed in this paper is valuable.

Table 10. Weight combination results in upper and lower layers.

Group	Upper-Layer Weight	Lower-Layer Weight	Count Cost	Distance Cost	Fairness Cost	Route Operating Cost
1	0.1	0.9	17.4	101.21	58.42	2439.26
2	0.2	0.8	17.7	97.89	57.09	2510.29
3	0.3	0.7	17.9	98.67	57.93	2543.40
4	0.4	0.6	18.1	95.48	56.12	2540.29
5	0.5	0.5	17.4	95.78	53.50	2480.77
6	0.6	0.4	17.9	93.66	54.82	2539.09
7	0.7	0.3	17.5	101.96	57.12	2537.14
8	0.8	0.2	17.7	97.81	56.08	2490.39
9	0.9	0.1	17.5	90.91	57.20	2475.09
	layered solution		17.0	100.78	61.32	2597.23

Considering the cost of the selected parcel-receiving station count, the cost of the average picking distance, the cost of picking fairness, and the cost of public air-route operation, the proportion of upper-layer model weight and lower-layer model weight are selected as 0.5 and 0.5. With this weight combination, the four costs of the bi-layer optimization model solved by GA-MMAS are the most balanced, where the cost of the upper-layer model is reduced by 5.12% on average, and the cost of the lower-layer model is reduced by 4.48%.

4.4. Time Complexity Analysis

In this paper, the nested GA-MMAS algorithm is used to solve the problem of logistics UAV parcel-receiving station location and public route planning. In general, it is considered that the time complexity of the genetic algorithm is $O(NG \times n^2)$, where NG is the maximum number of iterations of the genetic algorithm and n is the population size. The time complexity of the MMAS algorithm is $O(NC \times m \times n_s^2)$, where NC is the maximum number of iterations of MMAS, m is the population size, n_s is the number of cities, and, in this case, n_s is the number of selected stations. The time complexity of the GA-MMAS algorithm is the combination of the two algorithms. However, for different genetic algorithm individuals (location schemes), the selected station count is different, and the number of iterations of MMAS meeting the early-stop condition is also different, which will lead to a certain degree of difference in the time for each location scheme to use the MMAS algorithm to solve the public air-route planning scheme.

As shown in Figure 15, the station count in each generation of the genetic algorithm gradually decreases from 50 to about 25 with the algorithm iteration and fluctuates around 25. Therefore, taking five as the step length, the calculation time and iteration time of the MMAS algorithm when the selected station count is between 20 and 50 are analyzed. Each group was solved 100 times to obtain the average value, as shown in Table 11. It can be seen that when the selected station count in the location scheme is 20, the calculation time is only about 4.01 s, while when the station count is 50, the calculation time is as high as 24.21 s, which is consistent with the time complexity of the MMAS algorithm. When the average station count of the population is 50, it takes about 1800 s to calculate the public air-route operating cost of each individual in the population, and this kind of solution was not the optimal solution expected. If the method proposed in Section 3.2.3 is used, this part of the calculation can be avoided and the calculation time can be reduced.

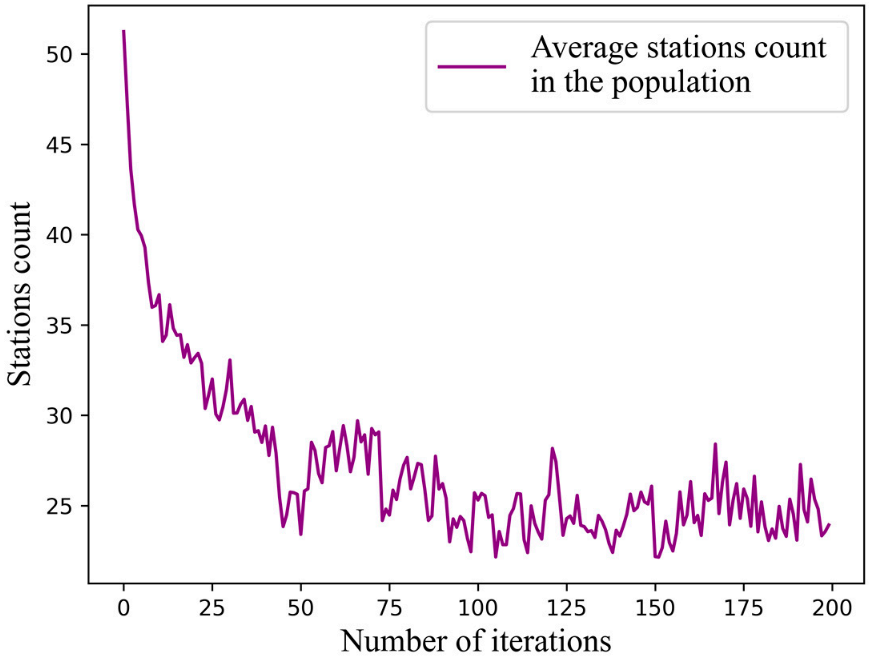

Figure 15. Average selected station count in each generation of the genetic algorithm.

Table 11. Weight combination results in upper and lower layers.

Station Count	20	25	30	35	40	45	50
Calculation time (s)	4.01	6.23	8.33	11.96	15.31	19.86	24.21
Iteration times (s)	32.89	34.00	32.48	35.23	35.01	36.42	36.45

5. Discussion

Based on the idea of bi-layer optimization, this paper solves the location problem of logistics UAV parcel-receiving stations and the planning problem of public air routes. The genetic algorithm is used to determine the UAV parcel-receiving station location combination among alternative locations, and the MMAS algorithm is used to determine the public air-route configuration, where the air route between nodes in a public air route is the result of the A* algorithm.

Simulation results show that the proposed logistics UAV parcel-receiving station location model and public air-route planning model are effective. The average cost of the upper-layer model and the lower-layer model is reduced by 5.12% and 4.48%, respectively, when the two models are combined into a bi-layer optimization model and solved using the nested GA-MMAS algorithm. It can be seen that the upper-layer model of parcel-receiving station location and the lower-layer model of public air-route planning influence each other, and the bi-layer optimization model proposed in this paper is valuable.

In the future, we will further study the construction method of the logistics UAV air-route network, add optional routes and alternative routes to public air routes, and improve the capacity and toughness of the logistics UAV transport air-route network. Another promising direction is to study the door-to-door logistics scenario, which can be further studied in combination with multi-level takeoff and landing points, parcel-receiving stations, and hub-and-spoke logistics networks.

Author Contributions: Conceptualization, H.Z.; methodology, F.W., D.F. and G.Z.; software, S.D. and C.D.; writing—original draft preparation, F.W.; writing—review and editing, J.Z. All authors have read and agreed to the published version of the manuscript.

Funding: This research was funded by the National Natural Science Foundation of China (71971114) and the Fundamental Research Funds for the Central Universities (No. NQ2022012).

Institutional Review Board Statement: Not applicable.

Informed Consent Statement: Not applicable.

Data Availability Statement: Not applicable.

Acknowledgments: The authors acknowledge with thanks the support for this work by the College of Civil Aviation at Nanjing University of Aeronautics and Astronautics.

Conflicts of Interest: The authors declare no conflict of interest.

References

1. Zhang, F. Status Quo and Future Prospects of UAV Industry. *Ind. Technol. Forum* **2020**, *19*, 14–15.
2. Zhang, H.H.; Li, S.; Yi, J.; Zhong, G. Review on Urban Low-Altitude Air Route Planning. *J. Nanjing Univ. Aeronaut. Astronaut.* **2021**, *53*, 827–838.
3. Shavarani, S.M.; Nejad, M.G.; Rismanchian, F.; Izbirak, G. Application of Hierarchical Facility Location Problem for Optimization of a Drone Delivery System: A Case Study of Amazon Prime Air in the City of San Francisco. *Int. J. Adv. Manuf. Technol.* **2018**, *95*, 3141–3153. [CrossRef]
4. Aurambout, J.P.; Gkoumas, K.; Ciuffo, B. Last Mile Delivery by Drones: An Estimation of Viable Market Potential and Access to Citizens Across European Cities. *Eur. Transp. Res. Rev.* **2019**, *11*, 1–21. [CrossRef]
5. Shavarani, S.M.; Golabi, M.; Izbirak, G. A Capacitated Biobjective Location Problem with Uniformly Distributed Demands in the UAV-supported Delivery Operation. *Int. Trans. Oper. Res.* **2021**, *28*, 3220–3243. [CrossRef]
6. Venkatesh, N.; Payan, A.P.; Justin, C.Y.; Kee, E.; Mavris, D. Optimal Siting of Sub-Urban Air Mobility (sUAM) Ground Architectures Using Network Flow Formulation. Available online: https://arc.aiaa.org/doi/abs/10.2514/6.2020-2921 (accessed on 8 June 2020).
7. Qian, X.Y.; Zhang, H.H.; Zhang, F.; Liu, H. Research on Location Allocation of UAV Landing Points for pacakge Distribution Logistics. *J. Wuhan Univ. Technol. (Transp. Sci. Eng.)* **2021**, *45*, 682–687+693.
8. Zhang, H.H.; Feng, D.K.; Zhang, X.W.; Liu, H.; Zhong, G.; Zhang, L.D. Urban Logistics Unmanned Aerial Vehicle Vertiports Layout Planning. *J. Transp. Syst. Eng. Inf. Technol.* **2022**, *22*, 207–214.
9. Liu, S.Q.; Zhang, J.; Li, G.Q. Location-Allocation Model of Logistics Distribution Network of Fast Fashion Products in Mature Period. *J. Southwest Jiaotong Univ.* **2012**, *47*, 333–340+354.
10. Chen, Y.Y.; Zhang, J.; Chen, Y.H.; Luo, J.Q. Research on Pickup Point Location Based on Customers' Bounded Rationality. *Ind. Eng. Manag.* **2015**, *20*, 92–100.
11. Chen, Y.Y.; Chen, Y.H. Research on Pickup Point Location Model and Algorithm in Presence of Gradual Coverage. *Appl. Res. Comput.* **2016**, *33*, 2275–2277+2297.
12. Han, X.; Zhang, J.; Chen, Y.Y. Multi-level Pickup Point Location Based on Customer Demand Heterogeneity. *Ind. Eng. Manag.* **2017**, *22*, 23–29+39.
13. Damilano, L.; Guglieri, G.; Quagliotti, F.; Sale, I.; Lunghi, A. Ground Control Station Eembedded Mission Planning for UAS. *J. Intell. Robot. Syst.* **2013**, *69*, 241–256. [CrossRef]
14. Yang, K.; Keat, G.S.; Sukkarieh, S. A Gaussian Process-based RRT Planner for the Exploration of an Unknown and Cluttered Environment with a UAV. *Adv. Robot.* **2013**, *27*, 431–443. [CrossRef]
15. Jayaweera, H.M.; Hanoun, S.; Sukkarieh, S. UAV Path Planning for Reconnaissance and Look-Ahead Coverage Support for Mobile Ground Vehicles. *Sensors* **2021**, *21*, 4595. [CrossRef]
16. Wu, Z.; Wu, H.L. UAV Route Planning Based on the Improved Genetic Algorithm. *Electron. Meas. Technol.* **2021**, *44*, 52–58.
17. Xu, C.C.; Liao, X.H.; Yue, H.Y.; Lu, M.; Chen, X.W. Construction of a UAV Low-altitude Public Air Route Based on an Improved Ant Colony Algorithm. *J. Geo-Inf. Sci.* **2019**, *21*, 570–579.
18. Jason, K.; Timonthy, W.; Michael, A. Learning Real—Time A* Path Planner for Unmanned Air Vehicle Target Sensing. *J. Area Comput.* **2006**, *3*, 108–122.
19. Song, Y.; Gu, H.J. UAV Route Planning Based on Improved A* Algorithm. *J. Chang. Univ. Technol.* **2020**, *41*, 579–601.
20. Zhang, H.H.; Li, H.; Liu, H.; Xu, W.W.; Zou, Y.Y. Path Planning for Logistics Unmanned Aerial Vehicle in Urban Area. *J. Transp. Syst. Eng. Inf. Technol.* **2020**, *20*, 22–29.
21. Mohammed, F.B.; Wanchao, C.; Wang, Z.; Huang, S.; Tan, D.Y.; Huang, T.; Low, K.H. Preliminary Concept of Adaptive Urban Airspace Management for Unmanned Aircraft Operations. In Proceedings of the AIAA Information Systems—AIAA Infotech at Aerospace, Kissimmee, FL, USA, 8–12 January 2018.
22. Zhang, X.N. Bi-level Optimization in Transportation Analysis. *J. Tongji Univ. Nat. Sci.* **2005**, *2*, 169–173.

23. Primatesta, S.; Rizzo, A.; la Cour-Harbo, A. Ground Risk Map for Unmanned Aircraft in Urban Environments. *J. Intell. Robot. Syst.* **2020**, *97*, 489–509. [CrossRef]
24. Ren, X.H.; Cheng, C.X. Construction and Application of Third-party Risk Model for Unmanned Aerial Vehicle Operation in Urban Environment. *China Saf. Sci. J.* **2021**, *31*, 15–20.
25. Zhang, H.H.; Hu, M.H. Multi-objection Optimization for Collaborative Scheduling Aircraft Landing on Multi-runways. *J. Southwest Jiaotong Univ.* **2009**, *44*, 402–409.
26. Li, S.; Zhang, H.H.; Li, Z.Z.; Liu, H. An Air Route Network Planning Model of Logistics UAV Terminal Distribution in Urban Low Altitude Airspace. *Sustainability* **2021**, *13*, 13079. [CrossRef]
27. Stützle, T.; Hoos, H.H. MAX–MIN Ant System. *Future Gener. Comput. Syst.* **2000**, *16*, 889–914. [CrossRef]
28. Xiang, Y.P.; Lei, A.H. The Location and Space Optimization of the Express Self-lifting Cabinet Based on the Perspective of the Delivery Efficiency and Customer Satisfaction: An Example of Houjiatang North, Changsha City in Hunan Province. *Econ. Geogr.* **2022**, *42*, 87–94.